Cross-shore decay of cliff top ground motions driven by local ocean swell and infragravity waves

Adam P. Young,[1] R. T. Guza,[1] Peter N. Adams,[2] William C. O'Reilly,[1] and Reinhard E. Flick[1]

Received 20 January 2012; revised 30 April 2012; accepted 17 May 2012; published 30 June 2012.

[1] Ground motions at the frequencies (between 0.01 and 0.1 Hz) of ocean infragravity and swell waves were observed on a cross-shore transect extending landward from the edge of a southern California coastal cliff. Cliff top ground motions are coherent and in phase with water level fluctuations at the cliff base. Vertical ground motions at infragravity and single frequencies decay rapidly with inland distance from the cliff edge (e-folding scale is about 12 m), and at the edge decrease by several orders of magnitude between high tide when waves reach the cliff base, and low tide when the waterline is about 50 m from the cliff base. The observed cross-shore decay scales are qualitatively consistent with gravitational loading and attraction of water waves at tidally modulated distances from the cliff base. At approximately constant distance from the waterline, ground motions vary roughly linearly with nearshore swell wave energy. In contrast to these locally forced ground motions, double frequency band (0.1–0.2 Hz) cliff top vertical ground motions are remotely generated with spatially uniform magnitudes approximately equal to those observed 14 km inland. Near the cliff edge, ground tilt dominates the observed large (relative to vertical) cross-shore acceleration at infragravity frequencies, contributes significantly to cross-shore acceleration at swell frequencies, and is a small fraction of cross-shore acceleration at higher frequencies.

Citation: Young, A. P., R. T. Guza, P. N. Adams, W. C. O'Reilly, and R. E. Flick (2012), Cross-shore decay of cliff top ground motions driven by local ocean swell and infragravity waves, *J. Geophys. Res.*, *117*, C06029, doi:10.1029/2012JC007908.

1. Introduction

[2] Ocean wave pressure fluctuations on the seafloor drive ground motions at frequencies of the incoming sea swell ("single frequency," here 0.04–0.10 Hz) at twice the sea swell frequency ("double frequency"), and at lower infragravity frequencies (here 0.01–0.04 Hz) (*Longuet-Higgins* [1950], *Haubrich et al.* [1963], *Haubrich and McCamy* [1969], *Kibblewhite and Wu* [1991], *Webb* [2007], and many others). The seafloor ground motions couple into seismic waves that propagate long distances. Shorter period ground shaking from wave impacts [*Adams et al.*, 2002], and longer period coastal ground translation and/or tilt from gravitational loading of ocean tides [*Farrell*, 1972; *Agnew*, 1997] and tsunamis [*Yuan et al.*, 2005; *Nawa et al.*, 2007] are also observed. Ocean related ground motions over a wide frequency band have been recorded on the deep ocean bottom [e.g., *Dolenc et al.*, 2005, 2007], shallow water ocean bottom [e.g., *Webb and Crawford*, 2010], at the coast [e.g., *Agnew and Berger*, 1978], and at large distances inland [e.g., *Bromirski*, 2001].

[3] Considered noise in many seismic studies, ocean generated ground motions are useful in studies of wave hindcasting [*Tillotson and Komar*, 1997; *Bromirski et al.*, 1999], ice shelf processes [*MacAyeal et al.*, 2006, 2009; *Cathles et al.*, 2009; *Bromirski et al.*, 2010], tsunamis [*Yuan et al.*, 2005], Earth hum [*Rhie and Romanowicz*, 2004, 2006; *Webb*, 2007; *Dolenc et al.*, 2008], crustal structure [*Crawford et al.*, 1991], and coastal cliff geomorphology [*Adams et al.*, 2002, 2005]. Other applications of seismic noise include forecasting volcanic eruptions [*Brenguier et al.*, 2008], detecting and characterizing mass movements [*Amitrano et al.*, 2005; *Suriñach et al.*, 2005], and measuring fluvial sediment transport [*Burtin et al.*, 2008; *Tsai et al.*, 2012].

[4] Here, new observations are used to estimate the dependence of locally forced coastal cliff top ground motions on tide level, incident wave conditions, and distance landward from the cliff edge. The observations are also used to develop simple, heuristic models for the cross-shore decay of ground motions, and to estimate cliff material strain magnitudes.

2. Background

[5] Detailed observations of cliff top ground motions and local ocean waves are relatively scarce. *Bossolasco et al.*

[1]Integrative Oceanography Division, Scripps Institution of Oceanography, University of California San Diego, La Jolla, California, USA.
[2]Department of Geological Sciences, University of Florida, Gainesville, Florida, USA.

Corresponding author: A. P. Young, Integrative Oceanography Division, Scripps Institution of Oceanography, University of California San Diego, 9500 Gilman Dr., La Jolla, CA 92093-0209, USA. (adyoung@ucsd.edu)

0148-0227/12/2012JC007908

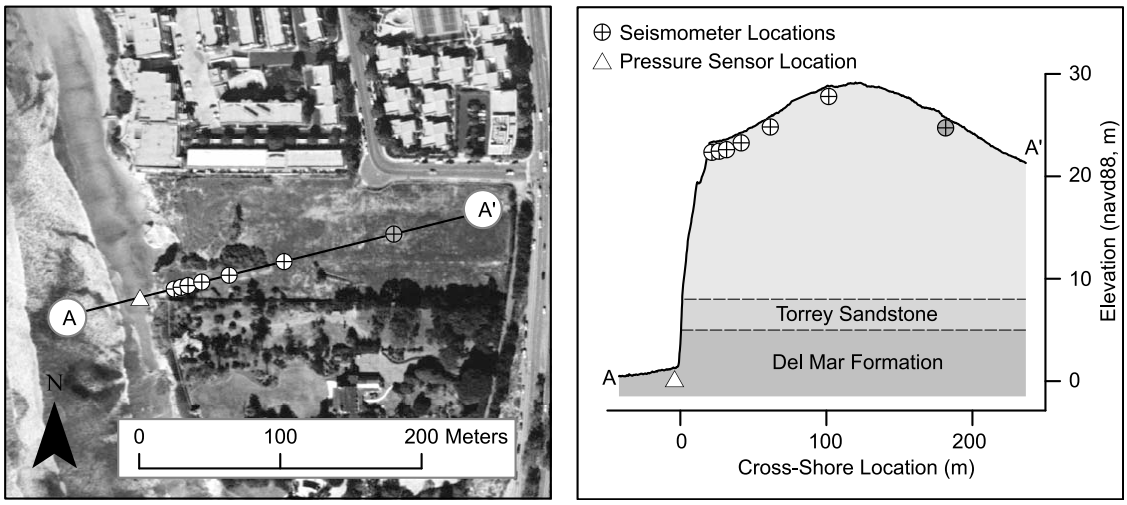

Figure 1. (left) Aerial view of study site. The cliffs are fronted by a narrow sand (and occasionally cobble) beach. Cliff top seismometer and cliff base pressure sensor locations, and transect end points A and A′, are shown. Ocean related seismic signals were relatively weak, and traffic noise relatively strong, at cross-shore location x = 160 m, and this locations is excluded from analysis. (right) Schematic cross-section and cliff composition. The lower unit, the Del Mar Formation, is an Eocene sedimentary deposit composed of sandy claystone interbedded with coarse-grained sandstone [*Kennedy*, 1975]. The overlying Torrey Sandstone is a massive coarse-grained and well-cemented Eocene sandstone. The upper cliff section is a weakly cemented, fine-grained sandy Pleistocene terrace deposit.

[1973] compared observations of microseisms at a coastal cliff with observations a few km inland, on the inland side of a harbor. At the coastal cliff, the spectral densities (i.e., energy level) of single and double frequency motions were approximately equal. At the harbor site, single frequency microseisms were weaker, ascribed to reduced ocean wave energy within the harbor.

[6] More recently, *Adams et al.* [2002] showed that the high frequency (1–25 Hz) wave-induced cliff shaking at a central California cliff, fronted by a gently sloping submerged shore platform, depended on offshore wave conditions, shelf bathymetry, and tide level. The high frequency shaking from wave impacts is accompanied by downward and seaward cliff "sway" as waves approach at the incoming sea swell frequency [*Adams et al.*, 2005]. Observations at the cliff edge, 12 m, and 30 m inland show cliff sway decreased with increasing distance landward from the cliff edge. *Adams et al.* [2005] suggested the associated longitudinal and shear strain, in the range of $0.5–4 \times 10^{-6}$ with each sea swell wave, potentially reduce the material strength of coastal cliffs through fatigue.

[7] *Pentney* [2010] observed ground motion in the 0.125–100 Hz range along a cross-shore transect with seismometer positions at the cliff top edge, 50 m, 200 m inland and at the base of a New Zealand cliff fronted by an elevated shore platform. Similar to previous studies, cliff ground motions increased with increasing incident wave height, decreased with distance inland, and were tidally modulated. However, in contrast with *Adams et al.* [2002, 2005], *Pentney* [2010] found that during large wave events, cliff top ground motion was lowest at high tide and greatest at mid-low tide, suggesting the cliff top motion was enhanced by wave energy dissipated at the seaward edge of the elevated shore platform. Dissimilar ground motions at the cliff base and top suggested the cliff structure influenced ground response. Distinct water elevations were also associated with an elevated cliff response at North Yorkshire, UK [*Lim et al.*, 2011], suggesting a local topographic (e.g., platform morphology, and/or structural) influence. Additional seismic studies of coastal cliffs [*Amitrano et al.*, 2005; *Senfaute et al.*, 2009] focused on non-ocean related signals including high frequency (40 Hz–10 kHz) seismic precursory patterns of cliff cracking and failure. At much lower frequencies (0.001–0.01 Hz, periods of 100–1000 s), *Agnew and Berger* [1978] suggested that the pressure loading and gravitational attraction of low frequency ocean waves cause vertical ground motions at coastal sites, including a southern California coastal cliff.

[8] Recently, *Young et al.* [2011] compared ground motions observed with a single seismometer located near the edge of a coastal cliff with water level fluctuations observed at the cliff base, and with ground motions observed 14 km inland. The present study extends that work by quantifying the dependence of locally driven (infragravity and single frequency) cliff top ground motions on tide level, incident wave energy, and setback distance from the cliff edge. Additionally, the contribution of ground tilt to the observed horizontal accelerations is estimated. The studied 20–30 m high cliff (Figure 1), located in northern Del Mar, California, USA, is described in detail in *Young et al.* [2011].

3. Methods

3.1. Seismometers

[9] Ground motions were measured at 100 Hz with three Nanometrics Compact Trillium broadband velocity seismometers at cross-shore cliff top positions located 0, 5, 10, 20, 40, 80, and 160 m from the approximate cliff top edge (22 m landward of the cliff base, Figure 1). Each position was occupied for approximately 2–4 weeks, between 1 November 2010 and 4 April 2011. Local traffic noise was relatively high

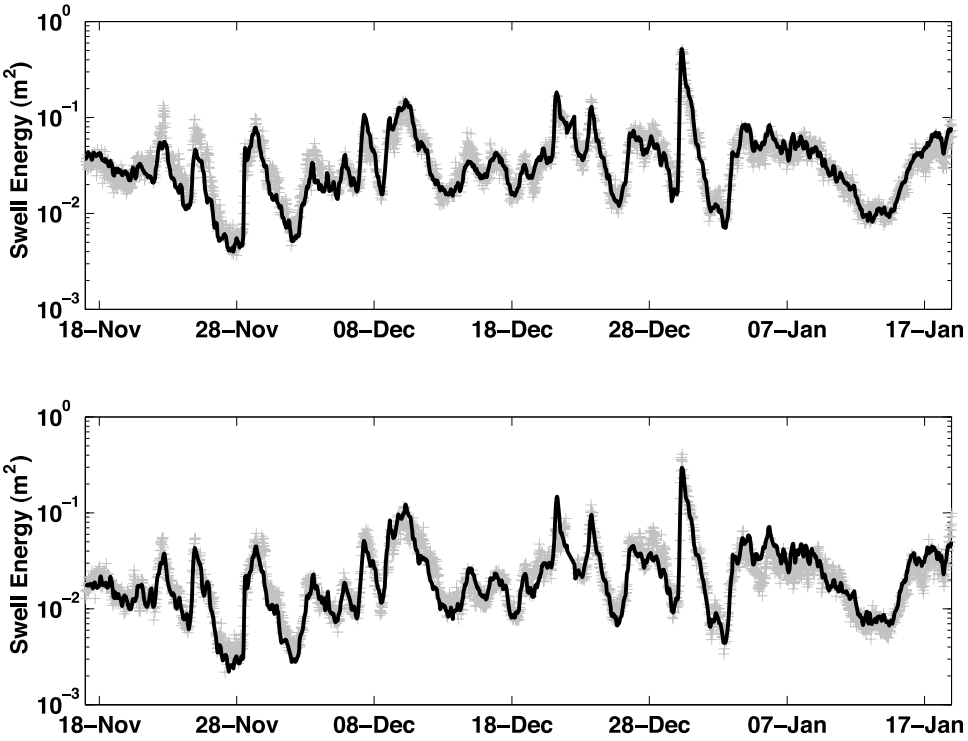

Figure 2. Modeled (black lines) and observed (gray crosses) swell energy (0.4–0.12 Hz) during the seismic observations versus time at (top) Torrey Pines Outer buoy (555 m water depth, approximately 6 km south of the study site) and (bottom) the San Elijo buoy (20 m water depth, approximately 6 km north of the study site).

for cross-shore position 160 m, and these observations are not considered below. Raw velocity measurements were phase and magnitude corrected in the frequency domain according to the manufacturer's (phase and amplitude) instrument response curve. Side-by-side deployments show similar energy spectra, and approximately 0 phase difference, for the range of frequencies considered here (0.01–1 Hz). Seismic data from the Camp Elliot (CPE) ANZA network seismometer (http://eqinfo.ucsd.edu/deployments/anza/index.php) located 14 km inland and 18 km southeast of the cliff site was analyzed and used for comparison. Time series originally in compass coordinates (E-W and N-S) were rotated (counterclockwise 14 degrees) into the approximate local shoreline orientation.

[10] Ground tilt maps part of the vertical gravitational acceleration onto the observed horizontal component of ground motions [*Rodgers*, 1968]. Tilt effects increase with increasing period, and can contribute significantly to horizontal accelerations at infragravity frequencies [*Webb and Crawford*, 1999; *Crawford and Webb*, 2000]. Tilt effects on the vertical component are generally considered negligible [*Graizer*, 2006]. Double-integration of the vertical and horizontal acceleration time series yields time series of vertical ground displacement and "apparent horizontal displacement" (that includes contributions from both displacement and tilt). Below, vertical ground motions are considered first (sections 4 and 5), with discussion of horizontal motions in section 6.

[11] Seismic and cliff base water levels, divided into one hour records, were detrended and processed with standard Fourier spectral methods, yielding spectral estimates with about 32 degrees of freedom [*Jenkins and Watts*, 1968]. Hours containing significant ground motion from earthquakes, post installation settlement, or local noise were removed manually. Seismic data was band-passed into infragravity (0.01–0.04 Hz), single (0.04–0.1 Hz), double (0.1–0.2 Hz), and high (0.2–0.5 Hz) frequency bands for analysis.

3.2. Incident (10 m Depth) Waves

[12] A wave buoy network [CDIP, http://cdip.ucsd.edu] was used to estimate hourly significant wave height at virtual buoys or "Monitored and Prediction" points (MOPS) seaward of the study area in 10 m depth at 100 m intervals along-shore. The effects of complex offshore (e.g., the Channel Islands) and local bathymetry on ocean swell (here 0.04–0.1 Hz, the same as the seismic single frequency band) were simulated with a spectral refraction wave model initialized with offshore buoy data [*O'Reilly and Guza*, 1991, 1993, 1998]. Seas (0.1–0.5 Hz) were estimated using nearby buoys and local bathymetry. Incident wave energy (10 m depth) was estimated as the mean of the five MOP locations closest to the cliff. Good model performance in the swell (0.04–0.10 Hz) frequency band is illustrated by comparison with observations at nearby (within 10 km of the cliff) buoys not used in modeling swell estimates (Figure 2).

4. Observations

4.1. Waves and Water Levels

[13] The spring tide range is about 2 m (Figure 3a). The distance from the cliff edge seismometer to the waterline

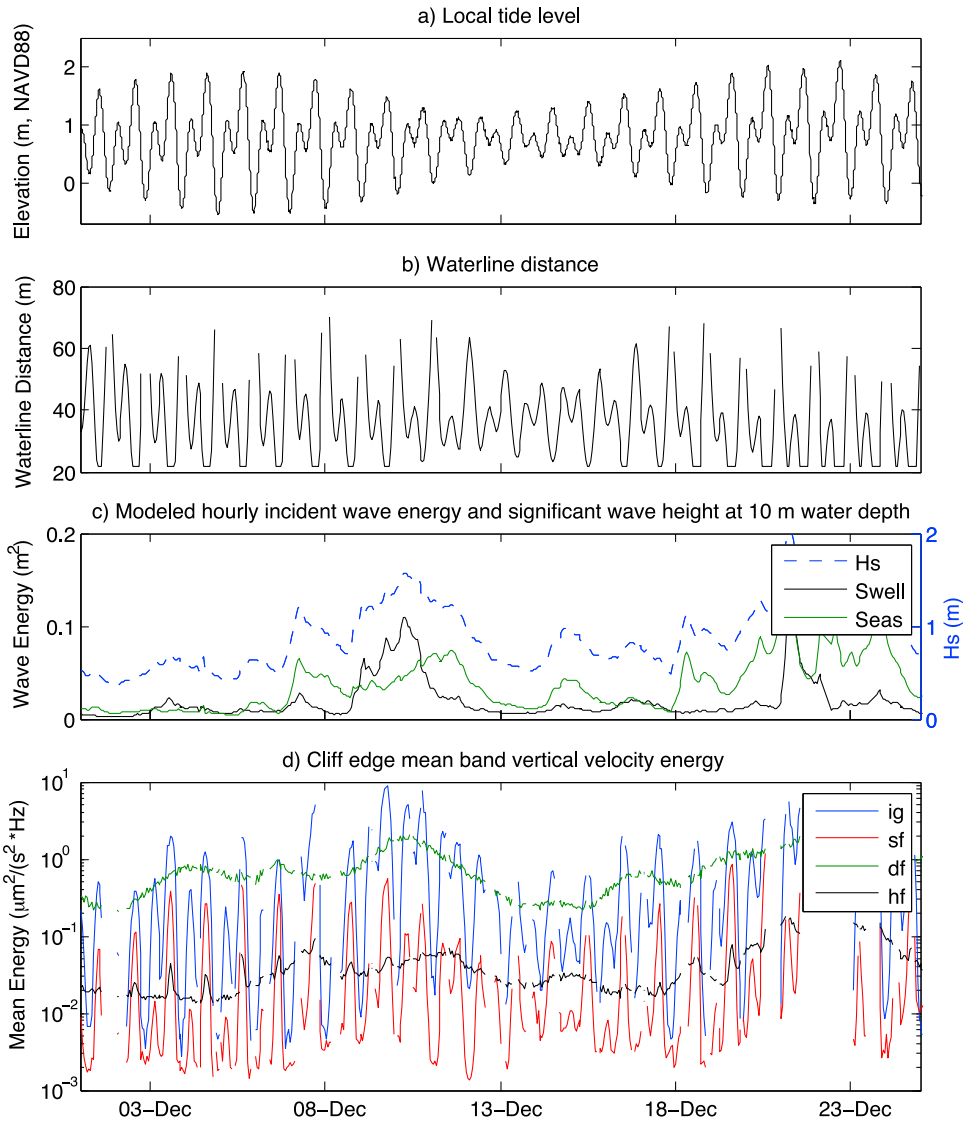

Figure 3. Time series (1–25 December, 2010) of (a) tide elevation measured at the Scripps pier, located a few km south of the study cliff (b) distance from the waterline to the cliff edge seismometer (located about 22 m landward of the cliff base, Figure 1), (c) right axis; hourly incident wave height *Hs* (sea + swell combined, blue dashed) and left axis; swell and sea band energies (black and green, respectively), modeled in 10 m depth, (d) band-averaged spectral density of vertical ground velocity in the infragravity (ig, 0.01–0.04 Hz), single frequency (sf, 0.04–0.10 Hz), double frequency (df, 0.1–0.2 Hz) and high frequency (hf, 0.2–0.5 Hz) bands.

varied between 22 m (when the waterline reached the cliff base, Figure 1), and about 80 m (Figure 3b). The waterline is defined as the cross-shore location where the mean hourly tide elevation (measured on a nearby pier) intersected the beach profile (based on interpolated approximately monthly surveys). In 10 m depth, wave heights based on combined swell and seas (0.04−0.3 Hz) ranged from about 30 cm to 3 m over the study period, with variable relative contributions from sea and swell (Figures 3c and 4b).

4.2. Cliff Edge Ground Motion

[14] Ground motions observed at the cliff edge are qualitatively similar to *Young et al.* [2011], at the same site. Increased tide level and incident wave energy increased cliff edge vertical ground motion at infragravity, single, and (to a lesser extent) high frequencies (Figures 3d and 4c). At double frequencies (0.1–0.2 Hz) spectral levels of vertical motions are nearly identical inland and at the cliff top (Figures 5a and 5e), consistent with a common (distant or spatially distributed) source.

[15] Spectral levels in cliff edge vertical velocity spectra at high tide are greatest in the locally generated infragravity band, whereas at low tide spectral maxima are usually in the remotely generated double frequency band (Figures 3d, 4c, 5a, and 5e). At high tide, cliff top ground motions in the infragravity, single frequency, and high frequency bands were generated locally by ocean waves at the cliff base. Cliff edge ground motion at incident swell and infragravity

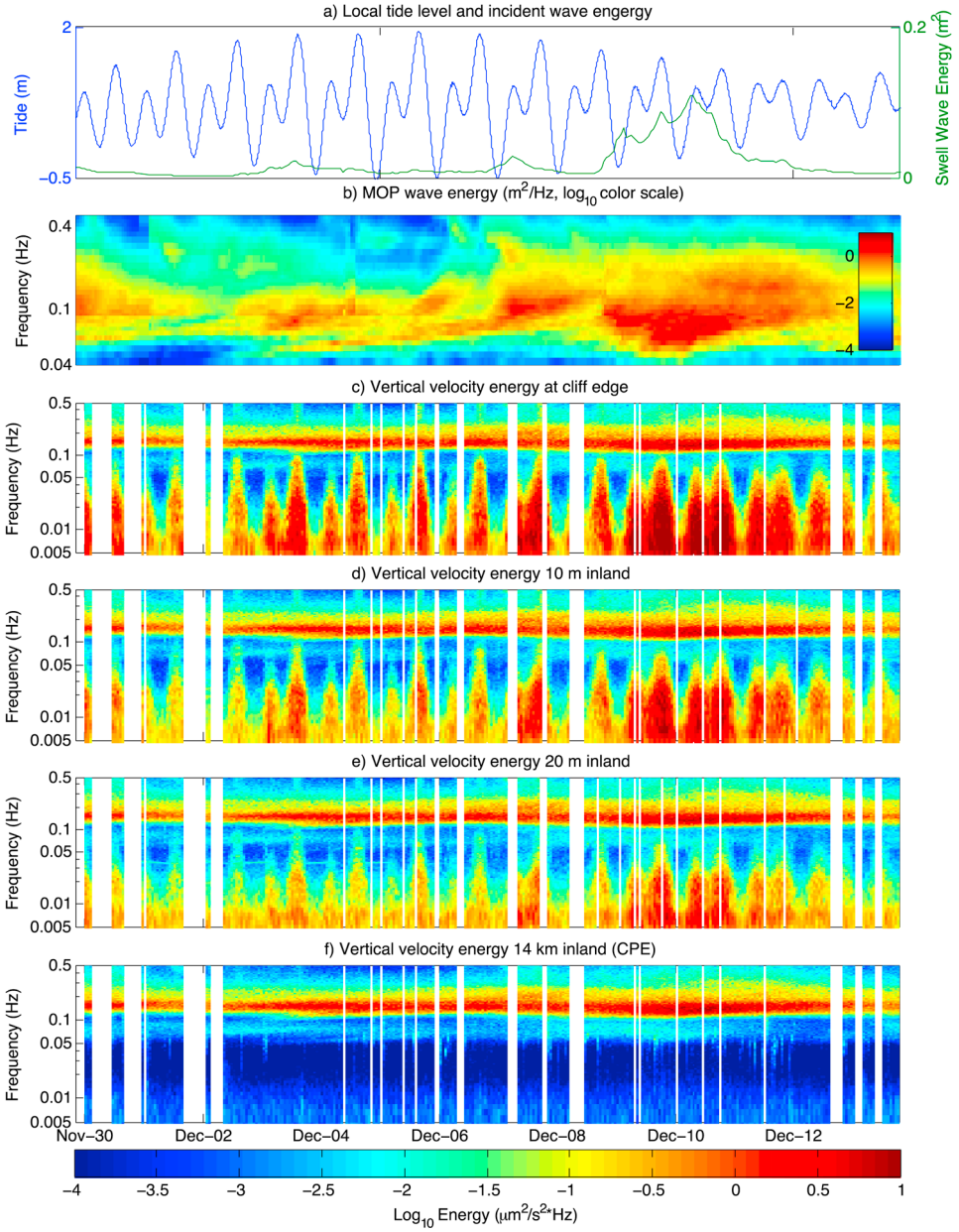

Figure 4. Time series (30 November to 19 December, 2010) of (a) tide elevation and swell wave energy, (b) 10 m depth wave energy spectral density, and vertical velocity energy density (see color scale) versus log frequency and time for the (c) cliff edge, 0 m, (d) cross shore position 10 m, (e) cross shore position 20 m, and (f) 14 km inland (Camp Elliot, CPE).

frequencies are highly coherent with, and in phase with, cliff base water level fluctuations (not shown). Spectral levels of ground motion at infragravity frequencies were sometimes higher than at single and double frequencies (Figure 5a), perhaps reflecting the dominance of infragravity waves inshoreline runup (e.g., swash) spectra observed when incident waves, energetic seaward of the surfzone, are dissipated by breaking during propagation across the surf zone [e.g., *Guza and Thornton*, 1982]. High frequency (0.2–0.5 Hz) shaking is caused by individual wave breaking and bores impacting the cliff. At low tide, energy levels of vertical ground motions at the cliff top decreased to inland levels at incident wave frequencies and higher (Figures 3, 4c, and 5e), and only infragravity-band motions were noticeably forced by local ocean waves.

4.3. Cross-Shore Variation

[16] During high tide, vertical ground motions at single and infragravity frequencies decayed with increasing distance inland from the cliff edge (compare cliff edge with 20 m further inland, Figures 4c and 4e) consistent with previous studies [*Adams et al.*, 2005; *Pentney*, 2010]. Vertical cliff top ground motion at the cliff edge was highly correlated with motions at other cross-shore locations less than about 80 m inland, with phase differences usually not detectably different from 0 (e.g., not larger than phase

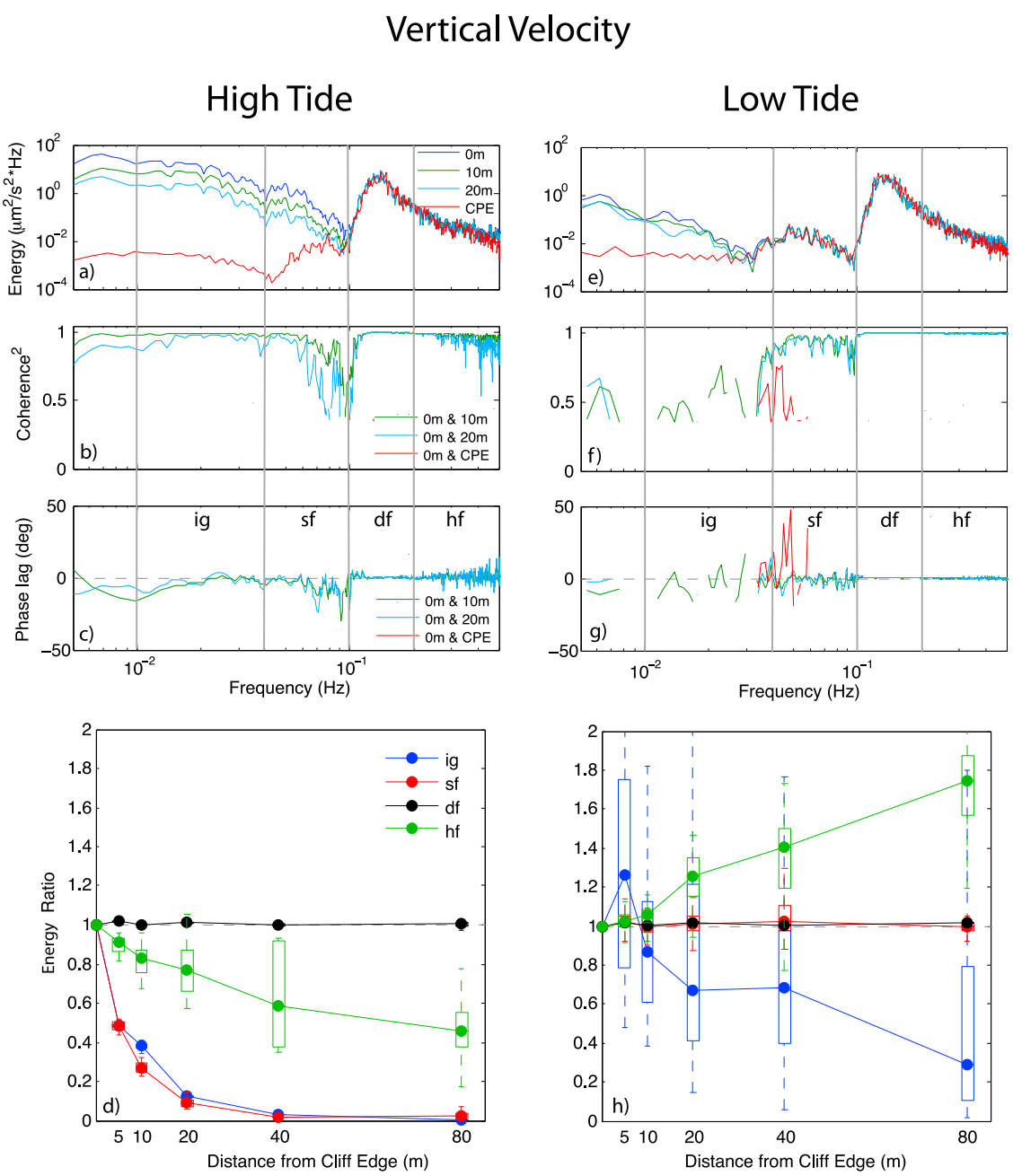

Figure 5. Energy spectral density, squared coherence (>95% significance), and phase lag between sites (see legends in Figures 5a–5c) versus frequency for a typical 1 h record of vertical velocity for (a, b, c) a high tide and (e, f, g) a low tide. Seismometers were located 0, 10, and 20 m from the cliff edge, and 14 km inland at CPE (see legends). Bottom panels are normalized (by the cliff edge observation) energy versus distance from cliff edge for (d) all high tides (level > 1.5 m) and (h) all low tides (level < 0.5 m). Boxplots show median (point), 25th and 75th percentiles (box), and range (whiskers). Single and double frequency bands at the cliff site contain significant nonlocal, teleseismic, background microseisms.

differences between side-by-side sensors, or expected owing to reduced coherence in the single frequency band, Figures 5b and 5c). The cross-shore decay of single frequency and infragravity band energies is strong and very similar, with weaker decay in the high frequency band (Figure 5d). Consistent with a remote source, cross-shore variation in the double frequency band is weak.

[17] During low tide, single frequency (as well as double frequency motions) energy levels decrease to inland values, with little cross-shore variation in energy across the cliff top (Figures 5e and 5h). Coherence between the cliff edge and the 14 km inland seismometer is statistically significant in the single frequency band (red in Figure 5f). High frequency motions at low tide decrease in energy toward the cliff edge, in contrast to high tide (compare green curves in Figures 5d

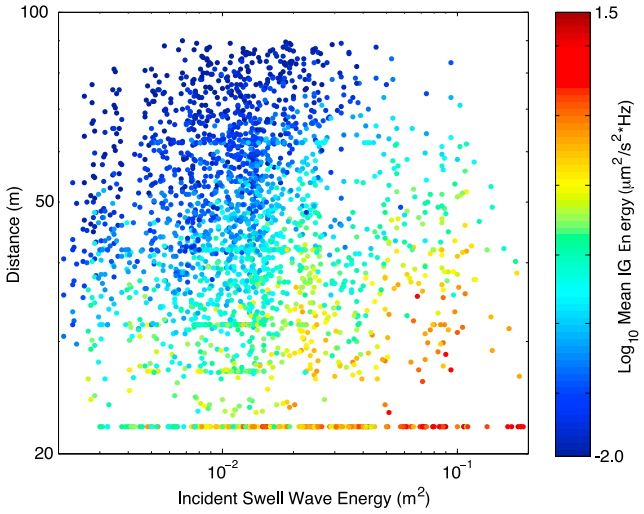

Figure 6. Hourly, mean infragravity vertical velocity energy density (colored dots, see scale) versus seismometer distance from the waterline and incident swell wave energy.

and 5h), consistent with an inland source (perhaps inland traffic noise at the right side of Figure 1, left panel). Infragravity frequencies generally decay with inland distance at low tide, but less severely and with greater scatter than at high tide (compare blue curves and associated scatter bars in Figures 5d and 5h). This scatter, and the reduced coherence between cliff top sensors, suggests noise is significant in the infragravity band during low tide.

5. Cross-Shore Decay Model

[18] Continuously fluctuating wave loading of the shore platform fronting the cliff drives cliff top ground motions at single [*Adams et al.*, 2005] and infragravity [*Young et al.*, 2011] frequencies. In response to runup of individual waves, the cliff tilted downward toward the ocean, as in the present observations (not shown). The observed vertical infragravity and single frequency band ground motions show similar cross-shore decay at high tide, with variance 20 m from the cliff edge reduced to about 10% of the cliff edge value (Figure 5d). The strong tidal modulation in energy, at a fixed sensor, also suggests a strong dependence on D, the distance from the water line. Observations from all tide levels illustrate the dependence of infragravity frequency ground motions on D and the incident swell wave energy (Figure 6).

[19] Assuming the ocean wave loading in the 100–1000 s range of periods is caused by strongly topographically trapped mode 0 edge waves, *Agnew and Berger* [1978] showed the loading and attraction components decay is approximately exponential in D. Later work focused on infragravity waves in the range considered here (periods 25–250 s) suggests a temporally varying mix of forced and free waves [*Herbers et al.*, 1994, 1995]. The observed directionally broad free infragravity wave spectrum results in offshore decay (h^{-1}) weaker than the exponential assumed by *Agnew and Berger* [1978], and stronger than the $h^{-1/2}$ predicted when refractive trapping is neglected. The spatial structure of infragravity wave energy within a km of the shoreline, where the contribution to gravitational loading and attraction on the cliff is maximum, depends on the free infragravity wave directional distribution, the magnitude of forced infragravity waves [*Herbers et al.*, 1994, 1995], and infragravity wave dissipation near the shoreline [*Senechal et al.*, 2011]. Quantitative modeling of infragravity loading is beyond the present scope.

[20] Cliff top seismometer observations are fit to two simple spatial decays; power law and exponential

$$E_{cliff\_IG} = c(E_{inc\_swell})^a (D)^b \quad (1)$$

$$E_{cliff\_IG} = r(E_{inc\_swell})^p e^{(-qD)} \quad (2)$$

where E_{cliff_IG} is the band-averaged spectral density of vertical velocity, E_{inc_swell} is the incident wave swell energy in 10 m depth (E_{inc_swell} (f) integrated between 0.04 and 0.1 Hz), and c, r are dimensional proportionality constants. A power law dependence of E_{cliff_IG} on E_{inc_swell} is assumed in both cases (*Herbers et al.* [1994, 1995] and many others). Observations show that shoreline infragravity energy levels depend more on the energy of incident swell waves than on the energy levels of higher frequency sea waves (*Okihiro and Guza* [1996], *Senechal et al.* [2011], and others), motivating the use of E_{inc_swell} in equations (1) and (2).

[21] Minimizing differences between observed and modeled infragravity band ground motions yields optimal power law (equation (1)) coefficients $a = 0.9$ and $b = -3.8$, with correlation of $r^2 = 0.86$ (Figure 7). Allowing for an additional 5% error, coefficients a and b could fall within 0.7 to 1.0, and -3.5 to -4.2 respectively. Calculations with different infragravity frequency boundaries (e.g., 0.006–0.05 Hz) and with seas (up to 0.3 Hz) included in E_{inc_swell}, yields results (not shown) with similar model exponents (a, b) and r^2.

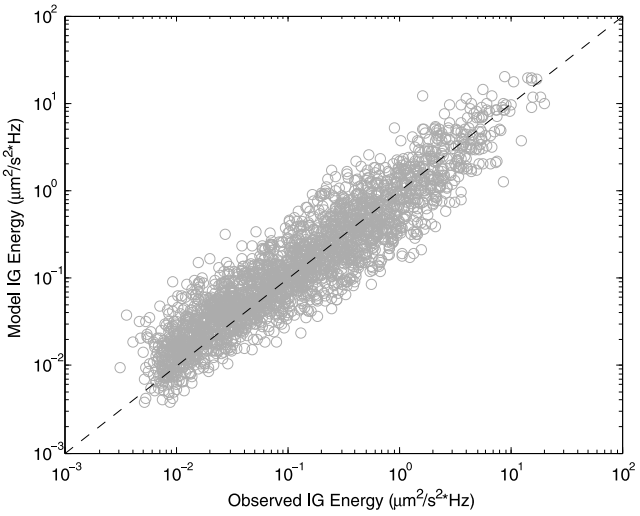

Figure 7. Parametric power law model fit ($a = 0.9$, $b = -3.8$, and $c = 1.1 * 10^7$ in equation (1)) versus observed hourly vertical velocity energy density averaged over the infragravity frequency band. Squared correlation between log model and log observed $r^2 = 0.86$. The seismometer self-noise estimated by the manufacturer was often reached at cross-shore location x = 80 m, and these observations (not shown) are excluded from the best fit.

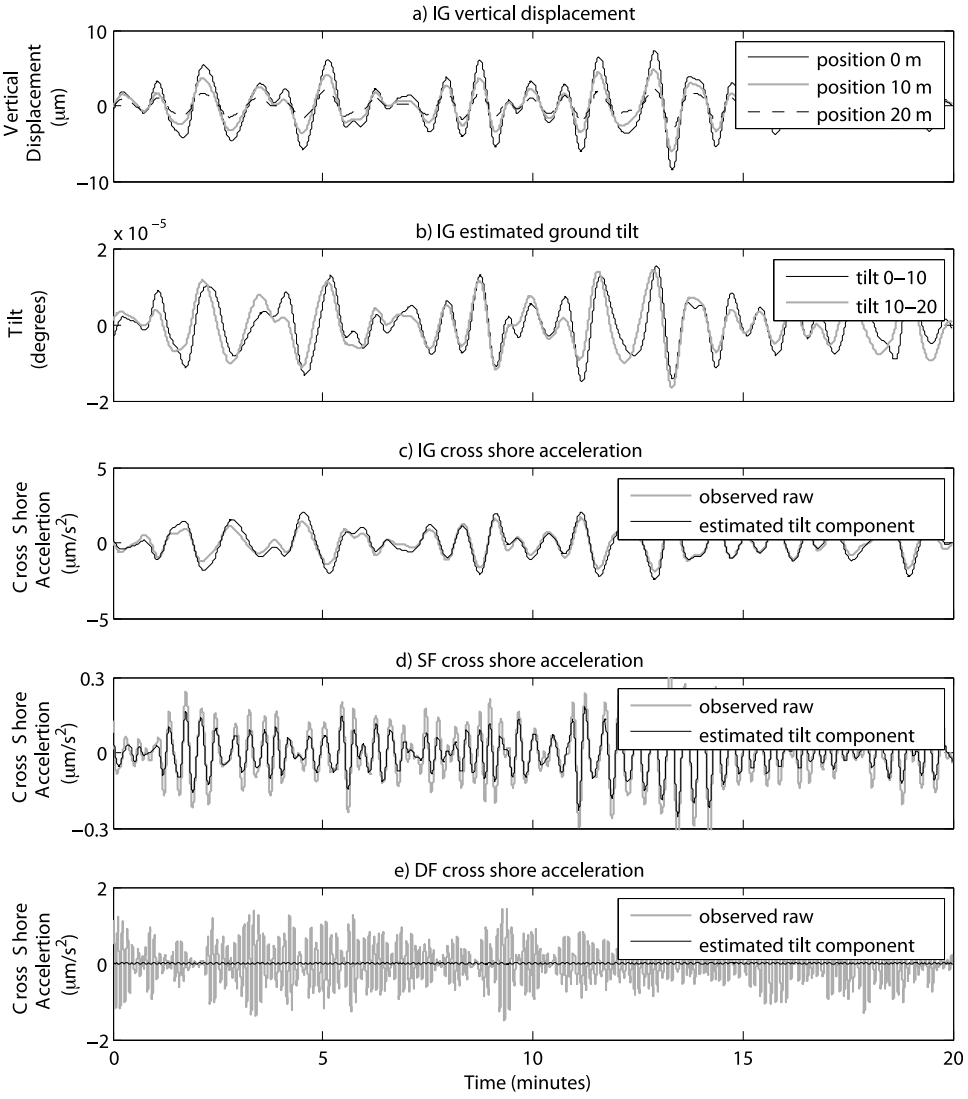

Figure 8. Time series of (a) infragravity band vertical ground displacements at cross shore locations 0 m, 10 m, and 20 m, (b) average ground tilt between sensors at locations 0 and 10 m, and 10 m and 20 m, (c, d, e) observed and estimated tilt component of cross-shore acceleration at location 10 m for infragravity, single, and double frequencies, respectively.

The best exponential fit (equation (2)) yields $p = 0.9$, $q = -0.08$, and $r = 233$, and (similar to the power law) $r^2 = 0.84$. The dependence E_{cliff_IG} on E_{inc_swell} ($a = p = 0.9$) is similar to the approximately linear dependence on E_{inc_swell} of free infragravity wave energy on the inner shelf [*Herbers et al.*, 1995]. The exponential model fit yields a 12.5 m e-folding distance. The cliff response to wave loading depends on the shear modulus and Poisson's ratio [*Agnew and Berger*, 1978], and may be enhanced by resonance at some frequencies. However, the detailed subsurface structure is unknown.

6. Ground Tilt and Cross-Shore Ground Motion

[22] The strong cross-shore decay of ground motions causes large tilt signals. Temporally fluctuating cross-shore ground tilt $d\eta/dx$, where η is the elevation of the ground in which the seismometer is embedded, maps gravity $g\ d\eta/dx$ into the cross-shore acceleration [*Rodgers*, 1968]. Tilt is in phase with the horizontal components of gravitational attraction and loading. At cross-shore position 5 m, $d\eta/dx$ is estimated using the difference between η observed at positions 0 m and 10 m, and at position 10 m using η observed at 0 m and 20 m (Figures 8a and 8b). The ratio of the estimated tilt component $g\ d\eta/dx$ to the observed cross-shore acceleration varies with frequency, and decreases from about 1.4 in the infragravity band to about 0.7 in the single frequency band, to less than 0.1 in the double frequency band (Figure 9). Values larger than 1.0 could be owing to errors in the tilt estimates based on differences. Spectra of ground apparent cross-shore velocity (Figure 10, the integrated horizontal acceleration) are similar to vertical velocity spectra (Figures 3, 4, and 5) in that infragravity and single frequency energy levels are strongly tidally modulated (Figures 10a and 10c) with strong landward decay at high tide (Figure 10b). In fact, in contrast to vertical velocity, at

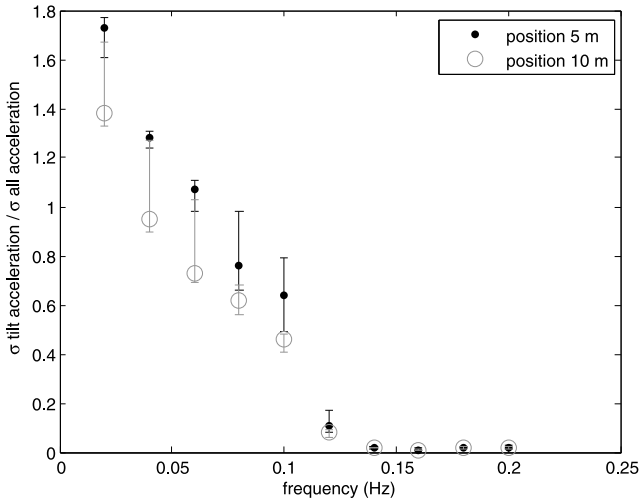

Figure 9. Ratio of the estimated tilt contribution to the total cross-shore standard deviation in 0.02 Hz wide frequency bands at positions 5 m (using sensors at 0 and 10 m from the cliff edge) and 10 m (using sensors at 0 and 20 m, Figure 8) during high tides (>1.5 m). Range bars show 25th and 75th percentiles. The tilt contribution decreases with increasing frequency, and approaches 0 in the double frequency band.

high tide even the double frequency band of cross-shore velocity decays with inland distance (compare black in Figure 5d and 10b), suggesting a local ocean source.

[23] At low tide, cliff top horizontal ground velocity spectra decrease substantially relative to high tide, but remain elevated compared with inland levels (Figure 10c). Infragravity cross-shore motions at low and high tide decay inland at similar rates (blue in Figures 10b and 10d), and cross-shore motions have much less scatter than vertical motions at low tide (blue in Figure 5h). Single frequency cross-shore motions generally decay with inland distance whereas vertical single frequency motions have constant cross-shore amplitude (compare red in Figures 5h and 10d). That is, compared with vertical motions, the cross-shore motions are more clearly dominated by an ocean source because the local ocean related signal is amplified by ground tilt.

[24] Tilt spectra E_{tilt} at each seismometer were estimated from the measured vertical spectra E_{vert} at that seismometer, and the empirical form for inland decay of the vertical signal (equation (1)),

$$E_{tilt} = E_{vert}\left(2\sigma^2 D/bg\right)^{-2} \tag{3}$$

where $\sigma = 2\Pi f$, D is the distance from the seismometer to the waterline, and b is the dimensionless exponent D^b in

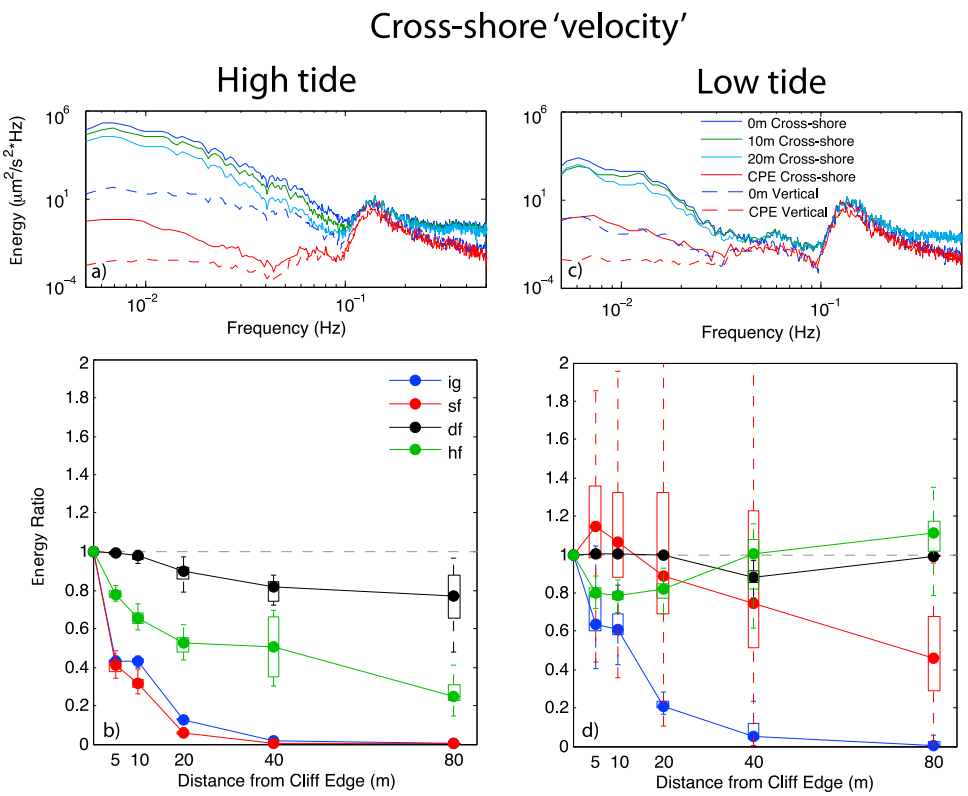

Figure 10. Energy spectral density versus frequency for a typical 1 h record of cross-shore velocity at (a) high tide and (c) low tide. Seismometers were located 0, 10, and 20 m from the cliff edge, and 14 km inland at CPE (see legends). Vertical energy spectral density (dashed lines, Figures 10a and 10c) are shown for comparison. Lower panels are normalized (by the cliff edge observation) energy versus distance from cliff edge for (b) all high tides (level > 1.5 m) and (d) all low tides (level < 0.5 m). Boxplots show median (point), 25th and 75th percentiles (box), and range (whiskers). Single and double frequency bands at the cliff site contain significant nonlocal, teleseismic, background microseisms.

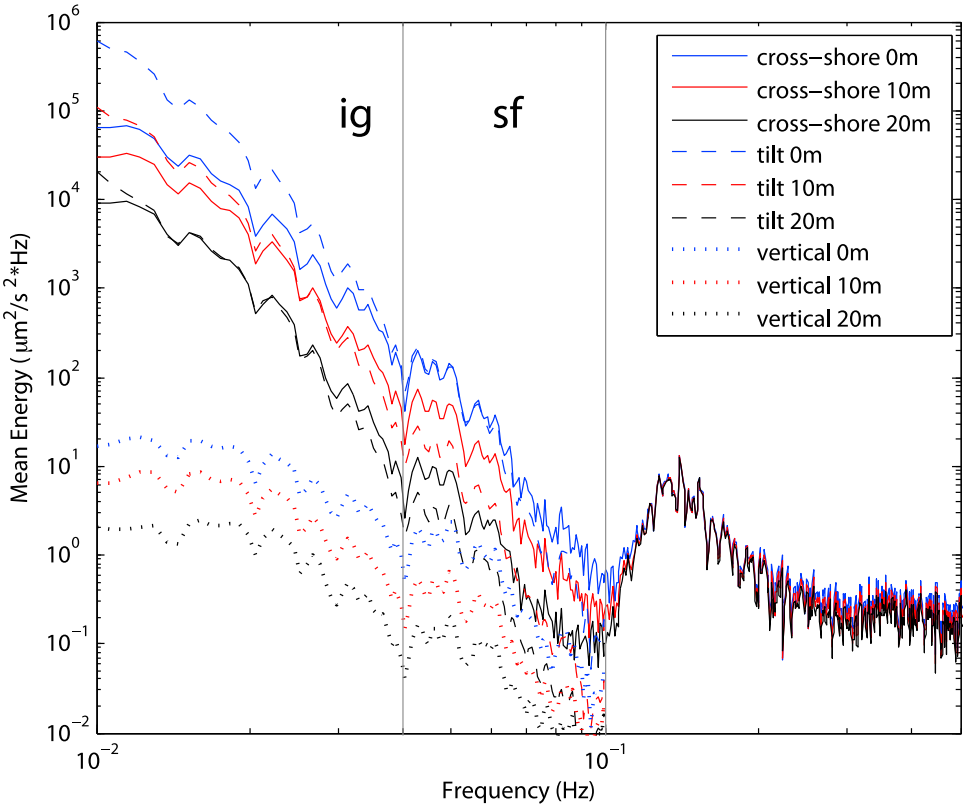

Figure 11. Energy density of apparent horizontal velocity observed (solid curves) and the tilt component (dashed curves) estimated using the observed vertical energy (dotted curves) and a power law decay model (equation (3), dashed curves) at 3 cliff top locations (see legend). These are 1 hr records with 32 degrees of freedom.

equation (1). The amplification (between vertical and horizontal tilt spectra) $(2\sigma^2 D/bg)^{-2}$ varies strongly with frequency. With D = 40 m and b = −3.8, $(2\sigma^2 D/bg)^{-2}$ varies between 10^4 for f = 0.01 Hz, and 1 for f = 0.1 Hz (compare vertical with tilt spectra in Figure 11). At infragravity frequencies (e.g., 0.01 Hz), the observed cross-shore spectra are dominated by the strongly amplified (10^4) tilt component, whereas at single frequencies the amplification of tilting is much reduced, and the tilt contribution is a much smaller fraction of the total signal. Similar conclusions concerning the contribution of tilt are reached using differences of adjoining sensors (Figures 8 and 9) and the empirical decay parameterization (equations (1) and (2)).

7. Geomorphic Perspective

[25] Observations of locally ocean generated cliff motion and cross-shore decay are generally consistent with previous studies [*Adams et al.*, 2002, 2005; *Pentney*, 2010; *Lim et al.*, 2011; *Young et al.*, 2011]. Cliff motion was tidally modulated with relatively more motion during elevated tidal levels consistent with observations at a cliff site with similar shore platform characteristics [*Adams et al.*, 2005]. However, the elevated high tide motion differs from sites with dissimilar platforms [*Pentney*, 2010; *Lim et al.*, 2011], suggesting that platform elevation and geometry influences ocean energy delivery to the cliffs.

[26] Ocean generated cliff motion decayed inland consistent with previous studies [*Adams et al.*, 2005; *Pentney*, 2010]. *Adams et al.* [2005] suggested cliff motion decay at sea swell frequency might cause cliff weakening through strain-related fatigue processes. The present observations of concurrent vertical displacements at different cross-shore locations yields estimates of vertical shear strain at ocean wave loading frequencies (0.01–0.1 Hz) that are largest near the cliff edge and decrease inland. The observed estimated strain magnitudes of 0.1–1 × 10^{-6} are similar in magnitude to 0.5–4 × 10^{-6} estimated by *Adams et al.* [2005]. Although these strain values are several orders of magnitude lower than typical ultimate strain values for rock, the continuous wave loading applies a high number of strain cycles and could potentially cause weakening through fatigue processes similar to thermal dilation. However, the cyclic strain magnitudes needed to cause fatigue damage are unknown.

8. Summary

[27] Ground motions at the frequencies (between 0.01 and 0.1 Hz) of ocean infragravity and swell waves were observed on a cross-shore transect extending landward from the edge of a southern California coastal cliff. During high tide, cliff top ground motions along the transect are coherent and in phase with one another, and with water level fluctuations at the cliff base. Vertical ground motions at infragravity and single frequencies decay rapidly with inland

distance from the cliff edge (e-folding scale is about 12 m), and at the edge decrease by several orders of magnitude between high tide, when waves reach the cliff base, and low tide, when the waterline is about 50 m from the cliff base. The observed cross-shore decay scales are qualitatively consistent with gravitational loading and attraction of water waves at tidally modulated distances from the cliff base. At approximately constant distance from the waterline, ground motions vary roughly linearly with nearshore swell wave energy. In contrast to these locally forced ground motions, double frequency band (0.1–0.2 Hz) cliff top vertical ground motions are remotely generated with spatially uniform magnitudes approximately equal to those observed 14 km inland. Near the cliff edge, ground tilt dominates the observed large (relative to vertical) cross-shore acceleration at infragravity frequencies, contributes significantly to cross-shore acceleration at swell frequencies, and is a small fraction of cross-shore acceleration at higher frequencies.

[28] **Acknowledgments.** Wave data collection was sponsored by the California Department of Boating and Waterways, and the U.S. Army Corps of Engineers, as part of the Coastal Data Information Program (CDIP). APY received research support from the California Department of Boating and Waterways Oceanography Program. The California Energy Commission PIER program funded the field observations. We thank the Del Mar Beach Club, the Solana Beach Lifeguards, and the Jacobs family for their assistance. Engineer Brian Woodward and his staff contributed substantially to the data collection. We also thank D. Amitrano and two anonymous reviewers for constructive remarks.

References

Adams, P. N., R. S. Anderson, and J. Revenaugh (2002), Microseismic measurement of wave-energy delivery to a rocky coast, *Geology*, *30*(10), 895–898, doi:10.1130/0091-7613(2002)030<0895:MMOWED>2.0.CO;2.

Adams, P. N., C. D. Storlazzi, and R. S. Anderson (2005), Nearshore wave-induced cyclical flexing of sea cliffs, *J. Geophys. Res.*, *110*, F02002, doi:10.1029/2004JF000217.

Agnew, D. C. (1997), NLOADF: A program for computing ocean-tide loading, *J. Geophys. Res.*, *102*(B3), 5109–5110, doi:10.1029/96JB03458.

Agnew, D. C., and J. Berger (1978), Vertical seismic noise at very low-frequencies, *J. Geophys. Res.*, *83*(B11), 5420–5424, doi:10.1029/JB083iB11p05420.

Amitrano, D., J. R. Grasso, and G. Senfaute (2005), Seismic precursory patterns before a cliff collapse and critical point phenomena, *Geophys. Res. Lett.*, *32*, L08314, doi:10.1029/2004GL022270.

Bossolasco, M., G. Cicconi, and C. Eva (1973), On mircoseisms recorded near a coast, *Pure Appl. Geophys.*, *103*(1), 332–346, doi:10.1007/BF00876409.

Brenguier, F., N. M. Shapiro, M. Campillo, V. Ferrazzini, Z. Duputel, O. Coutant, and A. Nercessian (2008), Towards forecasting volcanic eruptions using seismic noise, *Nat. Geosci.*, *1*(2), 126–130, doi:10.1038/ngeo104.

Bromirski, P. D. (2001), Vibrations from the "perfect storm", *Geochem. Geophys. Geosyst.*, *2*(7), 1030, doi:10.1029/2000GC000119.

Bromirski, P. D., R. E. Flick, and N. Graham (1999), Ocean wave height determined from inland seismometer data: Implications for investigating wave climate changes in the NE Pacific, *J. Geophys. Res.*, *104*(C9), 20,753–20,766, doi:10.1029/1999JC900156.

Bromirski, P. D., O. V. Sergienko, and D. R. MacAyeal (2010), Transoceanic infragravity waves impacting Antarctic ice shelves, *Geophys. Res. Lett.*, *37*, L02502, doi:10.1029/2009GL041488.

Burtin, A., L. Bollinger, J. Vergne, R. Cattin, and J. L. Nábělek (2008), Spectral analysis of seismic noise induced by rivers: A new tool to monitor spatiotemporal changes in stream hydrodynamics, *J. Geophys. Res.*, *113*, B05301, doi:10.1029/2007JB005034.

Cathles, L. M., E. A. Okal, and D. R. MacAyeal (2009), Seismic observations of sea swell on the floating Ross Ice Shelf, Antarctica, *J. Geophys. Res.*, *114*, F02015, doi:10.1029/2007JF000934.

Crawford, W. C., and S. C. Webb (2000), Identifying and removing tilt noise from low-frequency (<0.1 Hz) seafloor vertical seismic data, *Bull. Seismol. Soc. Am.*, *90*(4), 952–963, doi:10.1785/0119990121.

Crawford, W. C., S. C. Webb, and J. A. Hildebrand (1991), Seafloor compliance observed by long-period pressure and displacement measurements, *J. Geophys. Res.*, *96*(B10), 16,151–16,160, doi:10.1029/91JB01577.

Dolenc, D., B. Romanowicz, D. Stakes, P. McGill, and D. Neuhauser (2005), Observations of infragravity waves at the Monterey ocean bottom broadband station (MOBB), *Geochem. Geophys. Geosyst.*, *6*, Q09002, doi:10.1029/2005GC000988.

Dolenc, D., B. Romanowicz, R. Uhrhammer, P. McGill, D. Neuhauser, and D. Stakes (2007), Identifying and removing noise from the Monterey ocean bottom broadband seismic station (MOBB) data, *Geochem. Geophys. Geosyst.*, *8*, Q02005, doi:10.1029/2006GC001403.

Dolenc, D., B. Romanowicz, P. McGill, and W. Wilcock (2008), Observations of infragravity waves at the ocean bottom broadband seismic stations Endeavour (KEBB) and Explorer (KXBB), *Geochem. Geophys. Geosyst.*, *9*, Q05007, doi:10.1029/2008GC001942.

Farrell, W. E. (1972), Deformation of earth by surface loads, *Rev. Geophys.*, *10*(3), 761–797, doi:10.1029/RG010i003p00761.

Graizer, V. (2006), Tilts in strong ground motion, *Bull. Seismol. Soc. Am.*, *96*(6), 2090–2102, doi:10.1785/0120060065.

Guza, R. T., and E. B. Thornton (1982), Swash oscillations on a natural beach, *J. Geophys. Res.*, *87*(C1), 483–491, doi:10.1029/JC087iC01p00483.

Haubrich, R. A., and K. McCamy (1969), Microseisms–Coastal and pelagic sources, *Rev. Geophys.*, *7*(3), 539–571, doi:10.1029/RG007i003p00539.

Haubrich, R. A., W. H. Munk, and F. E. Snodgrass (1963), Comparative spectra of microseisms and swell, *Bull. Seismol. Soc. Am.*, *53*(1), 27–37.

Herbers, T. H. C., S. Elgar, and R. T. Guza (1994), Infragravity-frequency (0.005–0.05 Hz) motions on the shelf, Part I: Forced waves, *J. Phys. Oceanogr.*, *24*(5), 917–927, doi:10.1175/1520-0485(1994)024<0917:IFHMOT>2.0.CO;2.

Herbers, T. H. C., S. Elgar, R. T. Guza, and W. C. O'Reilly (1995), Infragravity-frequency (0.005–0.05 Hz) motions on the shelf, Part II: Free waves, *J. Phys. Oceanogr.*, *25*(6), 1063–1079, doi:10.1175/1520-0485(1995)025<1063:IFHMOT>2.0.CO;2.

Jenkins, G. M., and D. G. Watts (1968), *Spectral Analysis and Its Applications*, Holden-Day, San Francisco, Calif.

Kennedy, M. P. (1975), Geology of the San Diego metropolitan area, western area, *Bull. 200*, Calif. Div. of Mines and Geol., Sacramento, Calif.

Kibblewhite, A. C., and C. Y. Wu (1991), The theoretical description of wave-wave interactions as a noise source in the ocean, *J. Acoust. Soc. Am.*, *89*(5), 2241–2252, doi:10.1121/1.400970.

Lim, M., N. J. Rosser, D. N. Petley, and M. Keen (2011), Quantifying the controls and influence of tide and wave impacts on coastal rock cliff erosion, *J. Coastal Res.*, *27*(1), 46–56, doi:10.2112/JCOASTRES-D-09-00061.1.

Longuet-Higgins, M. S. (1950), A theory of the origin of microseisms, *Philos. Trans. R. Soc. Lond.*, *243*(857), 1–35, doi:10.1098/rsta.1950.0012.

MacAyeal, D. R., et al. (2006), Transoceanic wave propagation links iceberg calving margins of Antarctica with storms in tropics and Northern Hemisphere, *Geophys. Res. Lett.*, *33*, L17502, doi:10.1029/2006GL027235.

MacAyeal, D. R., E. A. Okal, R. C. Aster, and J. N. Bassis (2009), Seismic observations of glaciogenic ocean waves (micro-tsunamis) on icebergs and ice shelves, *J. Glaciol.*, *55*(190), 193–206, doi:10.3189/002214309788608679.

Nawa, K., N. Suda, K. Satake, Y. Fujii, T. Sato, K. Doi, M. Kanao, and K. Shibuya (2007), Loading and gravitational effects of the 2004 Indian Ocean tsunami at Syowa Station, Antarctica, *Bull. Seismol. Soc. Am.*, *97*(1A), S271–S278, doi:10.1785/0120050625.

Okihiro, M., and R. T. Guza (1996), Observations of seiche forcing and amplification in three small harbors, *J. Waterw. Port Coastal Ocean Eng.*, *122*(5), 232–238, doi:10.1061/(ASCE)0733-950X(1996)122:5(232).

O'Reilly, W. C., and R. T. Guza (1991), Comparison of spectral refraction and refraction-diffraction save models, *J. Waterw. Port Coastal Ocean Eng.*, *117*(3), 199–215, doi:10.1061/(ASCE)0733-950X(1991)117:3(199).

O'Reilly, W. C., and R. T. Guza (1993), A comparison of two spectral wave models in the southern California Bight, *Coastal Eng.*, *19*, 263–282, doi:10.1016/0378-3839(93)90032-4.

O'Reilly, W. C., and R. T. Guza (1998), Assimilating coastal wave observations in regional swell predictions. Part I: Inverse methods, *J. Phys. Oceanogr.*, *28*(4), 679–691, doi:10.1175/1520-0485(1998)028<0679:ACWOIR>2.0.CO;2.

Pentney, R. (2010), Seismic measurements of wave energy delivery to a rocky coastline: Okakari Point, Auckland, New Zealand, Master's thesis, Univ. of Auckland, Auckland, N. Z.

Rhie, J., and B. Romanowicz (2004), Excitation of Earth's continuous free oscillations by atmosphere-ocean-seafloor coupling, *Nature*, *431*(7008), 552–556, doi:10.1038/nature02942.

Rhie, J., and B. Romanowicz (2006), A study of the relation between ocean storms and the Earth's hum, *Geochem. Geophys. Geosyst.*, *7*, Q10004, doi:10.1029/2006GC001274.

Rodgers, P. W. (1968), Response of horizontal pendulum seismometer to rayleigh and love waves tilt and free oscillations of Earth, *Bull. Seismol. Soc. Am.*, *58*(5), 1384–1406.

Senechal, N., G. Coco, K. R. Bryan, and R. A. Holman (2011), Wave runup during extreme storm conditions, *J. Geophys. Res.*, *116*, C07032, doi:10.1029/2010JC006819.

Senfaute, G., A. Duperret, and J. A. Lawrence (2009), Micro-seismic precursory cracks prior to rock-fall on coastal chalk cliffs: A case study at Mesnil-Val, Normandie, NW France, *Nat. Hazards Earth Syst. Sci.*, *9*, 1625–1641, doi:10.5194/nhess-9-1625-2009.

Suriñach, E., I. Vilajosana, G. Khazaradze, B. Biescas, G. Furdada, and J. M. Vilaplana (2005), Seismic detection and characterization of landslides and other mass movements, *Nat. Hazards Earth Syst. Sci.*, *5*, 791–798, doi:10.5194/nhess-5-791-2005.

Tillotson, K., and P. D. Komar (1997), The wave climate of the Pacific Northwest (Oregon and Washington): A comparison of data sources, *J. Coastal Res.*, *13*(2), 440–452.

Tsai, V. C., B. Minchew, M. P. Lamb, and J.-P. Ampuero (2012), A physical model for seismic noise generation from sediment transport in rivers, *Geophys. Res. Lett.*, *39*, L02404, doi:10.1029/2011GL050255.

Webb, S. C. (2007), The Earth's 'hum' is driven by ocean waves over the continental shelves, *Nature*, *445*, 754–756, doi:10.1038/nature05536.

Webb, S. C., and W. C. Crawford (1999), Long-period seafloor seismology and deformation under ocean waves, *Bull. Seismol. Soc. Am.*, *89*(6), 1535–1542.

Webb, S. C., and W. C. Crawford (2010), Shallow-water broadband OBS seismology, *Bull. Seismol. Soc. Am.*, *100*(4), 1770–1778, doi:10.1785/0120090203.

Young, A. P., P. N. Adams, W. C. O'Reilly, R. E. Flick, and R. T. Guza (2011), Coastal cliff ground motions from local ocean swell and infragravity waves in southern California, *J. Geophys. Res.*, *116*, C09007, doi:10.1029/2011JC007175.

Yuan, X., R. Kind, and H. A. Pedersen (2005), Seismic monitoring of the Indian Ocean tsunami, *Geophys. Res. Lett.*, *32*, L15308, doi:10.1029/2005GL023464.